RSC Advances

PAPER

Cite this: *RSC Adv.*, 2014, **4**, 58362

Effective removal of Cr(VI) through adsorption and reduction by magnetic mesoporous carbon incorporated with polyaniline†

Guide Yang,[ab] Lin Tang,*[ab] Ye Cai,[ab] Guangming Zeng,*[ab] Pucan Guo,[ab] Guiqiu Chen,[ab] Yaoyu Zhou,[ab] Jing Tang,[ab] Jun Chen[ab] and Weiping Xiong[ab]

Received 9th August 2014
Accepted 21st October 2014

DOI: 10.1039/c4ra08432b

www.rsc.org/advances

Magnetic mesoporous carbon incorporated with polyaniline (PANI–Fe/OMC) is developed for enhanced adsorption and reduction of toxic Cr(VI) to non-toxic Cr(III). Several physicochemical techniques including TEM, FTIR and XPS analyses confirmed that magnetic iron nanoparticles and amino groups have been successfully bound on the mesoporous matrix. The adsorption capacity of the functionalized material is two- and ten-fold that of the magnetic mesoporous carbon (Fe/OMC) and pristine mesoporous silicon (SBA-15), respectively. Solution pH exhibited a remarkable impact on the Cr(VI) adsorption and the maximum uptake amount (172.33 mg g^{-1}) occurred at pH 2.0. The good fitting of adsorption process using pseudo-second-order and Langmuir models indicated the chemisorption process of Cr(VI) removal. The regeneration study revealed that PANI–Fe/OMC can be reused without loss of their activity in repetitive adsorption tests. Moreover, the resultant adsorbent can be effectively applied in actual wastewater treatment due to the excellent removal performance in fixed-bed column and real water samples. The interaction between Cr(VI) and PANI–Fe/OMC was investigated by FTIR and XPS analyses. The results indicate that the amino groups on the surface of PANI–Fe/OMC are involved in Cr(VI) uptake, and simultaneously some toxic Cr(VI) are reduced to non-toxic Cr(III) during the removal process.

1. Introduction

Chromium is a common contaminant in surface water and groundwater due to its widespread use in many industrial activities such as electroplating, leather tanning and pigmentation.[1] Depending on the pH levels, chromium most frequently occurs in two common oxidation states in wastewater: hexavalent chromium (Cr(VI)) and trivalent chromium (Cr(III)). Cr(III) is harmless and immobile in aqueous media, however, Cr(VI) is highly toxic, carcinogenic and mutagenic to all forms of living organisms.[2,3] The maximum permissible limit of Cr(VI) discharged in industrial effluents to surface water in China is 50 μg L^{-1}.[4] Consequently, it is indispensable to develop an economical, effective and reliable water treatment technique to remediate Cr(VI) contamination from water.

Conventional remediation techniques, including electrochemical precipitation, redox treatments, biological processes and ion exchange have been proposed to remediate Cr(VI)-contaminated wastewater. Of these, chemical precipitation is considered to be the most promising and economical method. This technique, however, produces large amounts of precipitate sludge that requires further treatment.[5] Although redox treatment is manoeuvrable and easy to implement, it needs a continuous energy and reagents supply.[6] Biological processes, on the other hand, exhibit low efficiency and require long operation times for effective treatment to be achieved.[7] Ion exchange is a simple approach to treat contaminated water, but only limited literature has been reported on the removal of Cr(VI). In addition, the relevant cost is higher than that of other methods as well.[8] By contrast, remediation of Cr(VI) contamination through adsorption is a promising technique because of its low cost, ambient conditions, high efficiency and simple operation.[9–11] Various adsorbents include activated carbons,[12] clays,[13] chitosan,[14] and polymeric resins[10] that have been applied for elimination of Cr(VI) in wastewater. However, several problems, including low adsorption capacity, slow process kinetics and poor mechanical strength are flaws which seriously affect the practical application of these adsorbents.

Recently, mesoporous materials have been widely investigated as promising candidates for various organic and metal ion removal processes because of their large pore volumes, high surface areas and excellent physical–chemical properties.[15,16] However, the large-scale application of mesoporous adsorbents is a challenge due to the costly separation process. Magnetic

[a]*College of Environmental Science and Engineering, Hunan University, Changsha, 410082, PR China. E-mail: tanglin@hnu.edu.cn; zgming@hnu.edu.cn; Fax: +86-731-88822778; Tel: +86-731-88822778*

[b]*Key Laboratory of Environmental Biology and Pollution Control (Hunan University), Ministry of Education, Changsha 410082, PR China*

† Electronic supplementary information (ESI) available. See DOI: 10.1039/c4ra08432b

separation has been proved to be an attractive technique for the fast separation rate, high efficiency, and simple and convenient experimental manipulation.[17,18] As a consequence, magnetic mesoporous adsorbent, as an excellent functional remediation material, has aroused increasing interest around the world. Polyaniline (PANI) is one of the most extensively used and studied conducting polymers. Due to its mechanical flexibility, environmental stability, easy synthesis and in-built amino groups, PANI has great advantages for wastewater treatment. The polymer not only can efficiently chelate with toxic Cr(VI) through electrostatic interactions, but also reduce fractional Cr(VI) to low toxicity Cr(III).[19,20] However, the regenerate and reuse of PANI is a challenge due to the small size of raw PANI. Therefore, it is requisite to incorporate PANI into support materials to overcome the disadvantages. To our best knowledge, only synthesis of PANI modified mesoporous carbon has been attempted, while research on preparation of functional mesoporous adsorbents combining the multiple advantages of mesoporous carbon, magnetic nanoparticles and PANI, as well as its excellent behavior for Cr(VI) removal has not been reported.

In this study, a novel functional adsorbent, magnetic mesoporous carbon incorporated with PANI, was prepared by *in situ* polymerization of aniline onto magnetic mesoporous carbon matrix. After systematic characterization of its structural properties, the resultant remediation material was applied for removal of Cr(VI) from water. Batch and fixed-bed experiments were used to investigate the adsorption behaviors of Cr(VI), and the kinetics, isotherms and thermodynamics were also utilized to evaluate the relevant Cr(VI) removal mechanisms. The effect of co-existing interferences and the regeneration of PANI–Fe/OMC were examined for its actual application. The interaction mechanisms between Cr(VI) and the modified mesoporous carbon were further explored.

2. Methods and materials

2.1 Prepared of PANI–Fe/OMC

Pluronic copolymer P123 ($EO_{20}PO_{70}EO_{20}$) was obtained from Sigma-Aldrich (USA). Solid humic acid (HA, 50–60% purity) was purchased from Acros Organics (Belgium) and solid fulvic acid (FA, 70% purity) was purchased from Shijiazhuang Lemandou Chemicals Co., Ltd. (China). The main elements of HA are: C 60.44%, H 3.53%, N 4.22%, O 31.31% and S 0.50%; and those of FA are: C 50.55%, H 4.12%, N 5.28%, O 39.56% and S 0.49%. Cross-polarization magic angle spinning ^{13}C NMR spectra of HA and FA were divided into four chemical shift regions: 0–50 ppm, 51–105 ppm, 106–160 ppm and 161–200 ppm. These regions were referred to as aliphatic, carbohydrate, aromatic and carboxyl regions. All other chemicals used were of analytical grade and were used without further purification. Aniline was distilled under vacuum before use. Stock solution of 1000 mg L^{-1} Cr(VI) was prepared from $K_2Cr_2O_7$. All stock solutions were prepared with high-purity water (18.25 MΩ cm, Milli-Q). Mesostructured SBA-15 silica template was prepared as follows according to the literature,[21] and magnetic mesoporous carbon (Fe/OMC) was synthesized as described previously with slight alterations.[22]

Modified magnetic mesoporous nanocomposite was obtained by oxidative polymerization of aniline.[23] Specifically, 2.0 mL of aniline was added into 400 mL of 0.2 M HCl solution, and then 1.0 g of Fe/OMC was added slowly under mechanical stirring. Following on it, ammonium persulfate (APS) with a molar ratio of aniline/APS of 1 : 1 was dissolved into 100 mL of 0.2 M HCl solution before adding to the above mixed solution. The *in situ* polymerization was carried out in an ice-water bath for 12 h continuous stirring. Then, the resultant solid was collected by magnetic separation and washed with high-purity water and ethanol several times. Finally, the desired product was obtained by drying in vacuum at 333 K overnight. Details about the preparation of SBA-15 and Fe/OMC are presented in ESI.†

2.2 Materials characterization

The synthesized samples were characterized before and after chemical modification by transmission electron microscopy (TEM), Brunauer–Emmett–Teller (BET) and Barrett–Joyner–Halenda (BJH) methods, Fourier transform-infrared techniques (FTIR), X-ray photoelectron spectra (XPS) and Zeta potential measurements. TEM images were obtained on a JEOL-1230 electron microscope operated at 100 kV (dot resolution: 0.24 nm and angle of inclination: ±20°). FTIR spectra were recorded with a Nicolet NEXUS 670 FTIR spectrometer by the standard KBr disk method. XPS analyses were conducted on an X-ray photoelectron spectroscope (Thermo Fisher Scientific, UK) with a resolution of 0.5 eV. BET and BJH measurements were carried out by a Micromeritics 2020 analyzer at 77 K. Zeta potential measurements *versus* pH have been collected using a Malvern ZEN3600 Zetasizer Nano.

2.3 Batch adsorption experiments and chemical analysis

Batch adsorption experiments of Cr(VI) were performed in duplicate in 50 mL sealed conical flasks on a shaker at 150 rpm. The pH of the suspension was adjusted by 0.1 M NaOH or HNO_3 solution. In each procedure, 10 mg of the PANI–Fe/OMC was added into 10 mL of Cr(VI) solution in desired concentration (10–500 mg L^{-1}) at pH 2.0. The suspension was reacted for 3 h to reach equilibrium, the used adsorbent was separated by applying an external magnetic field for 3 min. The initial and residual concentrations of Cr(VI) in the supernatants was analyzed using the 1,5-diphenylcarbazide method with a UV-vis spectrophotometer (UV-754N shanghai, China) at wavelength of 540 nm, and the corresponding total Cr was determined by a Perkin-Elmer Analyst 700 atomic absorption spectrophotometer (AAS, Perkin-Elmer, USA).

The adsorption capacity and the adsorption efficiency of PANI–Fe/OMC were calculated according to the following equations:

$$q_e = \frac{(C_0 - C_e) \times V}{W} \quad (1)$$

$$R(\%) = \frac{C_0 - C_e}{C_0} \times 100 \quad (2)$$

where q_e is the adsorption capacity of PANI–Fe/OMC towards Cr(VI) (or total Cr) (mg g^{-1}); C_0 and C_e are the initial and residual concentration of Cr(VI) (or total Cr) in solution (mg L^{-1}), respectively; V is the volume of the suspension (mL), W is the mass of adsorbent used (mg) and R(%) is the adsorption efficiency.

The effect of different interferences on Cr(VI) adsorption was studied. Specifically, 10 mg of the PANI–Fe/OMC was added into 10 mL of the solution containing 80 mg L^{-1} of Cr(VI) and desired concentrations of the interferents (Cl^-, NO_3^-, SO_4^{2-}, PO_4^{3-} HA or FA) (10–500 mg L^{-1}). After 3 h of reaction, the residual Cr(VI) was analyzed by AAS.

The regeneration studies of PANI–Fe/OMC were carried out in the batch process. Typically, 10 mL of 80 mg L^{-1} Cr(VI) solution was adsorbed first by 10 mg of PANI–Fe/OMC for 3 h to reach adsorption equilibrium. The used PANI–Fe/OMC was separated magnetically from the suspension and then washed thoroughly with ultrapure water to neutrality before desorbing with 10 mL of 0.1 M NaOH solution for 24 h. After magnetic separation and drying at 333 K overnight, the regenerative adsorbent was again used in the succeeding cycle.

2.4 Fixed-bed column experiments

Fixed-bed column tests were carried out at 298 K in three small polyethylene columns (10 mm diameter and 200 mm length). 1.0 g of SBA-15, Fe/OMC or PANI–Fe/OMC was put into each column, respectively. Then, the Cr(VI) solution with the initial concentration of 80 mg L^{-1} at pH 2.0 was pumped into each column in a down-flow direction using a peristaltic pump at the desired flow rate of 8 mL min^{-1}. The effluent samples were collected and the residual Cr(VI) was analyzed by the above UV-vis spectrophotometer.

3. Results and discussion

3.1 Characterization of PANI–Fe/OMC

The mesoporous structures of SBA-15 and PANI–Fe/OMC were characterized by the TEM technique (Fig. 1). Representative highly aligned stripe-like and hexagonally arranged structure with cylindrical pores was clearly observed, demonstrating that the resultant mesoporous materials possess well ordered 2D hexagonal mesostructures.[24] The black nanoparticles dispersed uniformly on the carbon matrix were magnetic iron particles. The isotherm curves of the as-synthesized nanoparticles (Fig. S1†) show typical type IV curves with broad capillary condensation steps at the relative pressure (P/P_0) of 0.4–0.8, indicating a narrow pore size distribution with uniform mesopores, which is further confirmed by the pore-size distribution profile from adsorption curve (Fig. S1 insert†). After the functionalization, decreases in surface area (374.89–55.95 m^2 g^{-1}) and pore volume (0.60–0.11 cm^3 g^{-1}) are distinctly observed (Table S1†). However, the pore diameter decreases slightly (4.81–4.74 nm), which is probably related to the fact that

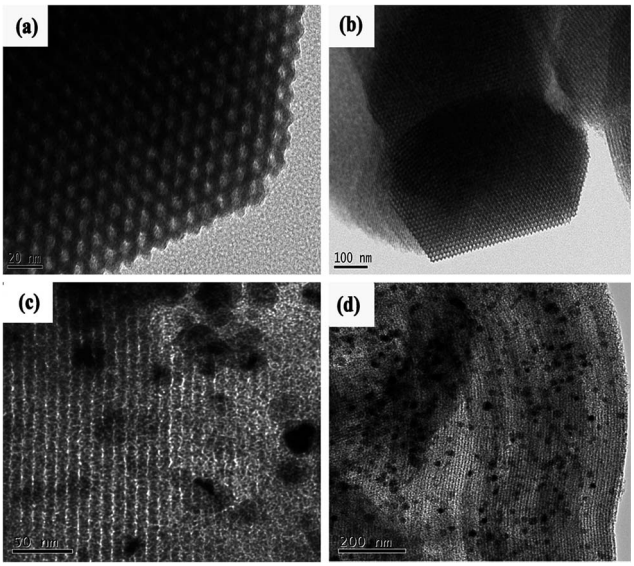

Fig. 1 TEM images of as-synthesized SBA-15 (a and b) and PANI–Fe/OMC (c and d).

functional groups are preferentially grafted near the pore entrances.[25]

The chemical compositions of mesoporous materials were characterized by FTIR (Fig. 2). The functional groups of the modified mesoporous material are significantly distinctive to those of the pristine mesoporous materials. Specifically, the strong peak around 3560 cm^{-1} corresponds to N–H stretching, and the two main bands at 1475 and 1592 cm^{-1} are related to the C=C stretching vibration modes of benzenoid and quinoid rings of PANI, corresponding to the extent of reduction and oxidation of PANI, respectively.[23] Meanwhile, the two C=C stretching vibration peaks also indicate that the resultant polyaniline is functionalized in the emeraldine salt form, capable of being further oxidized and reduced.[19] The peaks at 1302 and 1140 cm^{-1} can be assigned to C–N stretching and C–H in-plane bending of pernigraniline, respectively.[26] The weak adsorption peak at 567 cm^{-1} is attributed to the Fe–O stretch

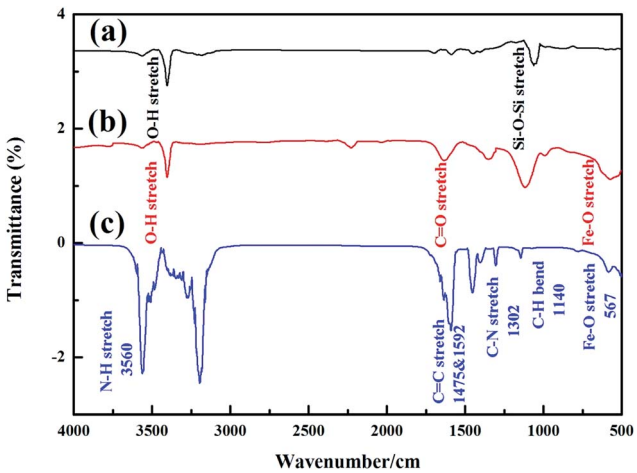

Fig. 2 FTIR spectra of SBA-15 (a), Fe/OMC (b), and PANI–Fe/OMC (c).

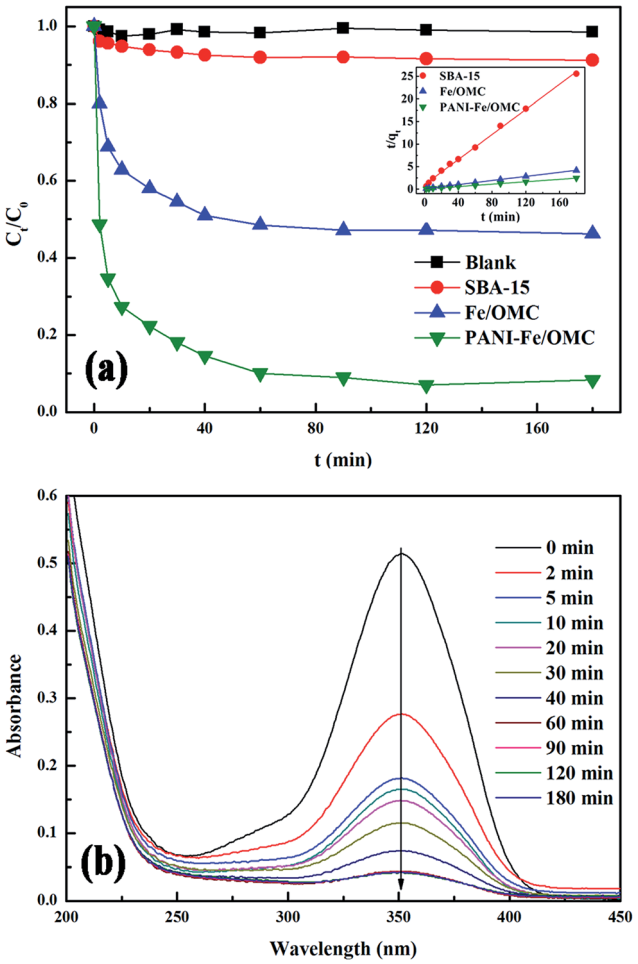

Fig. 3 Kinetics of Cr(VI) adsorption onto the PANI–Fe/OMC (a), where the inset is the pseudo second-order model for Cr(VI) adsorption; UV-vis absorption of the solutions after treatment with PANI–Fe/OMC as a function of contact time (b). Initial Cr(VI) concentration = 80 mg L^{-1}; pH = 5.0; T = 298 K.

vibration.[27] The survey XPS spectrum of the PANI–Fe/OMC is shown in Fig. S2a and b.† As expected, all the peaks assigned for carbon (C 1s), nitrogen (N 1s), iron (Fe 2p3) and oxygen (O 1s) can be clearly seen (Table S2†). After contact with Cr(VI), chromium (Cr 2p3) is also present in the spectrum (Fig. S2b†). The FTIR and XPS analyses have confirmed that PANI has been successfully polymerized on the mesoporous matrix.

Zeta potentials of both mesoporous materials were measured in a wide range of pH (from 2 to 11) and the corresponding results are presented in Fig. S3.† The isoelectric points (pH_{ZPC}) of the magnetic mesoporous material increased from 4.8 to around 10.0 after incorporation with PANI. The enhanced isoelectric points of PANI–Fe/OMC could yield stronger electrostatic attraction between nanoparticles and Cr(VI) anions, and thus the chromium uptake efficiencies would increase.

3.2 Adsorption kinetics

Adsorption of Cr(VI) on three different mesoporous adsorbents as a function of contact time is presented in Fig. 3a. As seen, the Cr(VI) adsorption on PANI–Fe/OMC exhibited an initial rapid adsorption followed by a slow removal rate that gradually reached equilibrium. Adsorption equilibrium was reached within 120 min, and the equilibrium adsorption efficiency of PANI–Fe/OMC reached 92%, which is approximately two- and ten-folds as high as that of Fe/OMC and SBA-15, respectively. Since the specific surface area of PANI–Fe/OMC was 55.95 m^2 g^{-1}, smaller than Fe/OMC (374.89 m^2 g^{-1}) and SBA-15 (575.21 m^2 g^{-1}), the micropore adsorption of Cr(VI) is negligible, and the excellent adsorption behavior by PANI–Fe/OMC was probably related with the introduction of amine groups. A large number of amine groups on the PANI–Fe/OMC surface offered additional affinity and more available binding sites for Cr(VI), accelerating the uptake of Cr(VI). The spectrophotometric techniques were used to characterize the Cr(VI) adsorption process, the Cr(VI) showed a characteristic peak at 350 nm in the UV-vis absorption curve (Fig. 3b).[28] The peak gradually slowed down with time from 0 to 180 min, and reflected well the adsorption behavior of PANI–Fe/OMC. To make validate the adsorption process, two kinetic models, the pseudo-first-order and the pseudo second-order models were used to describe the kinetics of Cr(VI) adsorption. The relevant equations of eqn (3) (pseudo-first-order model) and eqn (4) (pseudo-second-order model) are as follows:

$$\frac{dq_t}{dt} = k_1(q_e - q_t) \quad (3)$$

$$\frac{dq_t}{dt} = k_1(q_e - q_t)^2 \quad (4)$$

where q_e and q_t (mg g^{-1}) are the adsorption capacities of PANI–Fe/OMC at equilibrium and time t (min), respectively, k_1 (min^{-1}) and k_2 (g mg^{-1} min^{-1}) are the related rate constants, respectively. The fit of the pseudo-second-order model is presented in the inset of Fig. 3a, and the corresponding two model parameters are listed in Table 1. As can be seen, the pseudo-second-order model could better fit the adsorption process with a higher correlation coefficient (R^2 > 0.99), suggesting that the

Table 1 Adsorption kinetic model parameters for the adsorption of Cr(VI) onto three different mesoporous adsorbents

	Pseudo-first-order model			Pseudo-second-order model			
Adsorbents	k_1 (min^{-1})	$q_{e,cal}$ (mg g^{-1})	R^2	k_2 (g mg^{-1} min^{-1})	$q_{e,cal}$ (mg g^{-1})	R^2	$q_{e,exp}$ (mg g^{-1})
SBA-15	0.154	6.18	0.859	0.0189	7.20	0.997	7.04
Fe/OMC	0.177	39.86	0.945	0.0047	44.13	0.999	43.02
PANI–Fe/OMC	0.351	68.58	0.938	0.0046	74.96	0.999	74.38

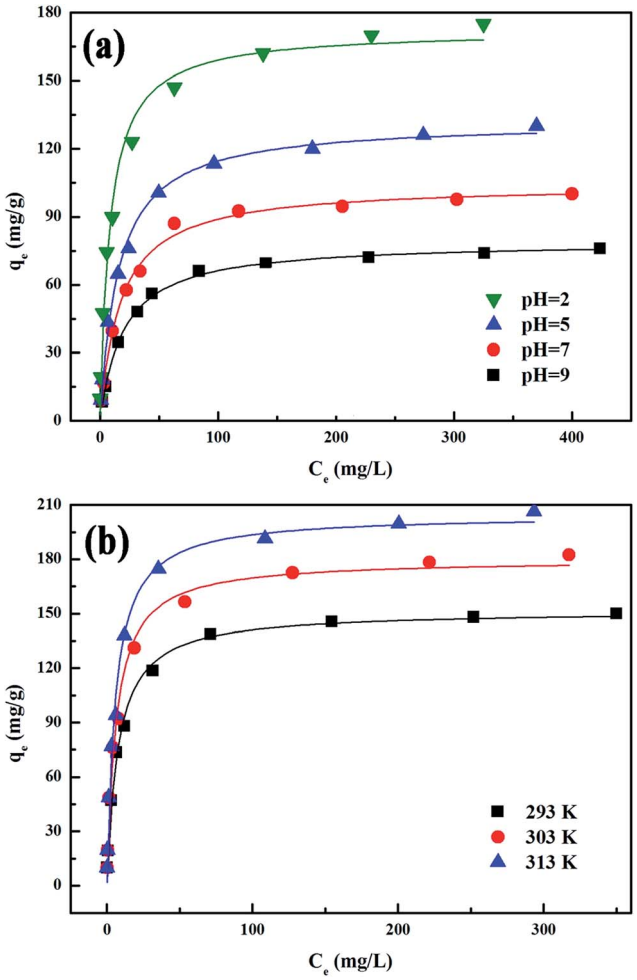

Fig. 4 The isotherms of Cr(VI) adsorption onto PANI–Fe/OMC at different pH values (a) and temperatures (b).

Cr(VI) adsorption was involved in the chemisorption rate-controlling mechanism.[29]

3.3 Effect of pH

Fig. 4a shows Cr(VI) adsorption on PANI–Fe/OMC as a function of pH in different initial Cr(VI) concentrations at 298 K. It indicates that the adsorption capacity declined with the increase of pH, and the maximum uptake amount attained is approximately 172 mg g^{-1} at pH 2.0. Compared with just over 79 mg g^{-1} of uptake amount at pH 9.0, the solution pH demonstrated a significant effect on Cr(VI) removal. This phenomenon is related to the surface property of the mesoporous adsorbent. Since the pH_{ZPC} of PANI–Fe/OMC is around 10.0, the surface charge of the PANI–Fe/OMC at pH < pH_{ZPC} is positive due to the protonation reaction. Obviously, lower pH can lead to a more positive charge on the surface of the adsorbent, and thus anionic species of Cr(VI), such as $Cr_2O_7^{2-}$, CrO_4^{2-}, and $HCrO_4^-$, can easily be adsorbed onto the PANI–Fe/OMC surface because of the electrostatic attraction.[10] Eqn (5) and (6) indicates the protonation of the amino groups in PANI–Fe/OMC and the reaction between the protonated adsorbent and Cr(VI). With pH increase, the available positively charged adsorption sites decreased gradually; consequently, only a handful of Cr(VI) could be removed by the nanoparticles.

$$R\text{–}NH_2 + H^+ \rightarrow R\text{–}NH_3^+ \quad (5)$$

$$2R\text{–}NH_3^+ + Cr_2O_7^{2-} \rightarrow R\text{–}NH_3^+\text{–}Cr_2O_7^{2-}\text{–}H_3^+N\text{–}R \quad (6)$$

Isothermal adsorption is a requisite to expound the adsorption process. In the study, two typical isotherm adsorption models—Langmuir and Freundlich models—are applied to fit the isothermal adsorption data. The relevant equations are expressed in eqn (7) and (8):

$$q_e = \frac{q_{max} K_L C_e}{1 + K_L C_e} \quad (7)$$

$$q_e = K_F C_e^{1/n} \quad (8)$$

where q_{max} (mg g^{-1}) is the maximum amount of adsorption corresponding to complete monolayer coverage, q_e (mg g^{-1}) and C_e are the equilibrium adsorption capacity and equilibrium Cr(VI) concentration, K_L (L mg^{-1}) is the Langmuir constant related to adsorption energy, K_F is the Freundlich related to the sorption capacity, and n is the constant representing adsorption intensity. The adsorption isotherm is represented in Fig. 4a and the relevant parameters calculated from the Langmuir and Freundlich isotherm models are listed in Table 2. It was noticeable that the Langmuir model with a correlation of over

Table 2 Langmuir and Freundlich isotherm parameters for the adsorption of Cr(VI) onto PANI–Fe/OMC at different pH values and temperatures

		Langmuir			Freundlich		
Conditions		K_L (L mg^{-1})	q_{max} (mg g^{-1})	R^2	K_F	n	R^2
pH values	pH 2.0	0.120	172.33	0.988	46.45	4.08	0.935
	pH 5.0	0.065	132.15	0.995	47.30	5.65	0.857
	pH 7.0	0.058	104.27	0.994	36.14	5.56	0.859
	pH 9.0	0.051	79.18	0.998	26.25	5.41	0.863
Temperatures	293 K	0.134	151.60	0.994	44.66	4.42	0.897
	303 K	0.165	180.04	0.986	53.87	4.36	0.919
	313 K	0.176	204.56	0.988	62.18	4.38	0.913

Table 3 Comparison of Cr(VI) uptake capacity of various adsorbents

Adsorbent	Q_m (mg g^{-1})	Equilibrium time (min)	pH	T (K)	References
Polyaniline coated ethyl cellulose	38.76	30	1.0	303	19
N-doped porous carbon with magnetic particles	30.96	30	3.0	298	30
Aluminum magnesium mixed hydroxide nanoparticles	112.00	150	4.0	313	31
Fe@Fe_2O_3 core–shell nanowires	7.78	300	6.4	298	32
PEI-modified magnetic adsorbent	78.13	30	2.0	298	33
Poly(2-ethylaniline)/chitosan	147.16	240	3.0	298	34
Ficus carica fiber based activated carbon	44.84	105	3.0	303	35
Modified magnetic mesoporous silica MCM-48	115.60	90	4.0	298	36
Amino-functionalized mesoporous alumina	59.50	60	2.0	298	37
Mesoporous magnetic carbon nanocomposite	3.74	10	—	298	38
PANI–Fe/OMC	172.33	120	2.0	298	This study

0.98 gave a better fit to the equilibrium data. The results are in agreement with previous studies for Cr(VI) adsorption,[9,30] and it is assumed that the adsorption of Cr(VI) onto PANI–Fe/OMC was mainly chemisorption. A comparison has been made between the resultant PANI–Fe/OMC and previously reported adsorbents for Cr(VI) adsorption (Table 3).[19,30–38] The results of the analyses demonstrated that this novel functional adsorbent gains advantage over many other adsorbents, indicating that PANI–Fe/OMC is a fairly promising candidate for the treatment of chromium-containing wastewater.

In order to determine how Cr(VI) interacts with PANI–Fe/OMC, the total chromium concentration was measured at pH 2.0 and the result is shown in Fig. S4.† Cr(VI) removal could be distinguished from the total Cr, indicating that Cr(VI) was not entirely removed by adsorption, and simultaneously, a significant portion of Cr(VI) was reduced to Cr(III).[39] The Cr(VI) removal is an adsorption-couple reduction process.

3.4 Thermodynamic of adsorption

Fig. 4b shows the effect of temperature on Cr(VI) adsorption onto the PANI–Fe/OMC at pH 2.0. The adsorption isotherms of Cr(VI) onto the modified mesoporous adsorbent at different temperatures were also listed in Table 2. The adsorption capacity of PANI–Fe/OMC increased from 151.60 mg g^{-1} to 204.56 mg g^{-1} with a temperature increase from 283 K to 303 K, which demonstrated that the Cr(VI) adsorption was better at higher temperatures.[40] Additionally, thermodynamic parameters such as free energy change (ΔG), enthalpy change (ΔH) and entropy change (ΔS) were exploited to explore the further interaction, and the relative thermodynamics equations are expressed as follows:

Table 4 Thermodynamic parameters for the adsorption of Cr(VI) onto PANI–Fe/OMC at different temperatures

Temperatures	K_L (L mol^{-1})	ΔS^0 (J K^{-1} mol^{-1})	ΔH^0 (kJ mol^{-1})	ΔG^0 (kJ mol^{-1})
293 K	6968	109.42	10.45	−2.16
303 K	8580			−2.27
313 K	9152			−2.38

$$\ln K_L = \frac{\Delta S}{R} - \frac{\Delta H}{RT} \quad (9)$$

$$\Delta G = \Delta H - T\Delta S \quad (10)$$

where K_L is the Langmuir constant (L mol^{-1}), R is the ideal gas constant (8.314 J mol^{-1} K^{-1}) and T is the absolute temperature (K). ΔH and ΔS are calculated from the slope and intercept of the linear plots of ln K_L *versus* 1/T. The ΔG, ΔH, and ΔS values are listed in Table 4. The negative ΔG values indicate that the Cr(VI) uptake processes were thermodynamically feasible and spontaneous under the experimental conditions.[41] The positive value of ΔH^0 (10.45 kJ mol^{-1}) for Cr(VI) adsorption confirmed the endothermic nature of adsorption, and the positive value of ΔS^0 (109.42 J mol^{-1} K) suggests an increased randomness occurring at the solid solution interface during the adsorption process.

3.5 Effect of co-existing interferents

In the natural environment, Cr(VI) often co-exists with other inorganic and organic substances, which may compete for

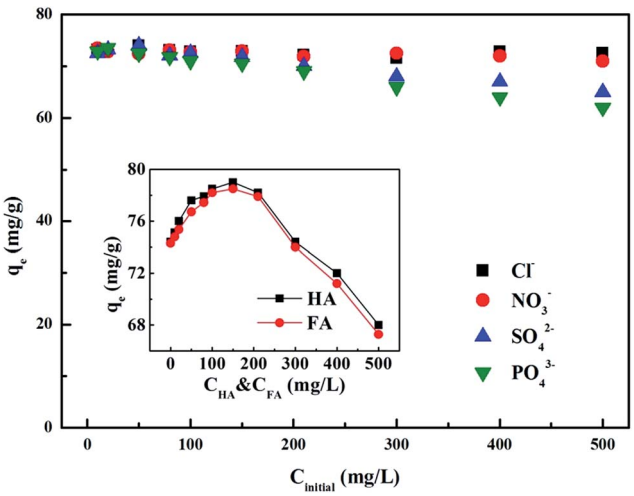

Fig. 5 The effect of co-existing anions on Cr(VI) adsorption, the inset shows the effect of organic matter.

adsorption sites and decrease the Cr(VI) removal efficiency of the PANI–Fe/OMC. Based on this, the effect of commonly co-existing interferents is investigated in this study.

3.5.1 Inorganic interferents. Fig. 5 presents the effect of common anions on Cr(VI) adsorption with the initial Cr(VI) concentration of 80 mg L^{-1} at 298 K. As the concentration of additional interferents increased, the Cr(VI) removal capacity almost remains steady in the solution containing monovalent Cl^- or NO_3^- anion, while it exhibited a slight decrease under divalent SO_4^{2-} or trivalent PO_4^{3-} anions. This is because compared with monovalent Cl^- and NO_3^- anions, the physicochemical properties of SO_4^{2-} and PO_4^{3-} anions are more similar to Cr(VI) oxyanions, that is, with almost equivalent ion sizes and structures,[9] and thus these anions may compete with Cr(VI) for available adsorption sites. Thus, SO_4^{2-} and PO_4^{3-} anions are more influential than Cl^- and NO_3^- anions. Given the lower limited concentrations of SO_4^{2-} and PO_4^{3-} in natural water (0–5 mg L^{-1}),[42] the interference from sulfate and phosphate were almost insignificant.

3.5.2 Organic interferents. The effect of co-existing organic substances on the adsorption of Cr(VI) are investigated and shown in the inset of Fig. 5. The existence of the two organic interferents, HA and FA, can accelerate Cr(VI) adsorption at lower concentrations, while an obvious suppression occurs at higher interferent concentrations. The promotion impact suggests HA and FA may act as a scavenger for the uptake of Cr(VI). On the one hand, large amounts of Cr(VI) were adsorbed on the PANI–Fe/OMC surface, and on the other hand, HA and FA were firstly adsorbed onto the original adsorption sites on the PANI–Fe/OMC surface, and then the fraction of the residual Cr(VI) interacted with the new adsorption sites caused by HA and FA adsorption.[43] Thus, the Cr(VI) removal amount was enhanced under lower HA and FA concentrations. While at higher HA and FA concentrations, these extra additives might compete with Cr(VI) for the adsorption sites on the resultant sample, such as amine groups, thus resulting in a decrease in the uptake of Cr(VI).

3.6 Regeneration of PANI–Fe/OMC

Regeneration and reuse tests were conducted to regenerate used PANI–Fe/OMC using 0.1 M NaOH in Fig. S5.† The result demonstrates the adsorption activity of PANI–Fe/OMC deteriorated with the increase in the number of reuse cycles, but only very slightly. The adsorption efficiency could still reach 90% on the seventh reuse cycle, which demonstrated that PANI–Fe/OMC was capable of being regenerated and reused effectively.

3.7 Fixed-bed column adsorption

Column studies were used to examine the performance of the three adsorbents to remove Cr(VI) from water (Fig. 6a). As expected, the uptake of Cr(VI) through SBA-15 and Fe/OMC columns showed the poor performance, and the saturation adsorption capacities of Cr(VI) were only less than 240 and 640 bed volumes (BV), respectively, much less than that of PANI–Fe/OMC with 1300 BV of saturation sorption amount. Furthermore, three different real water environments, including ultrapure water, tap water and river water were used to evaluate the adsorption behavior of PANI–Fe/OMC (Fig. 6b). It indicated that the uptake capacities of Cr(VI) were slightly limited in tap water

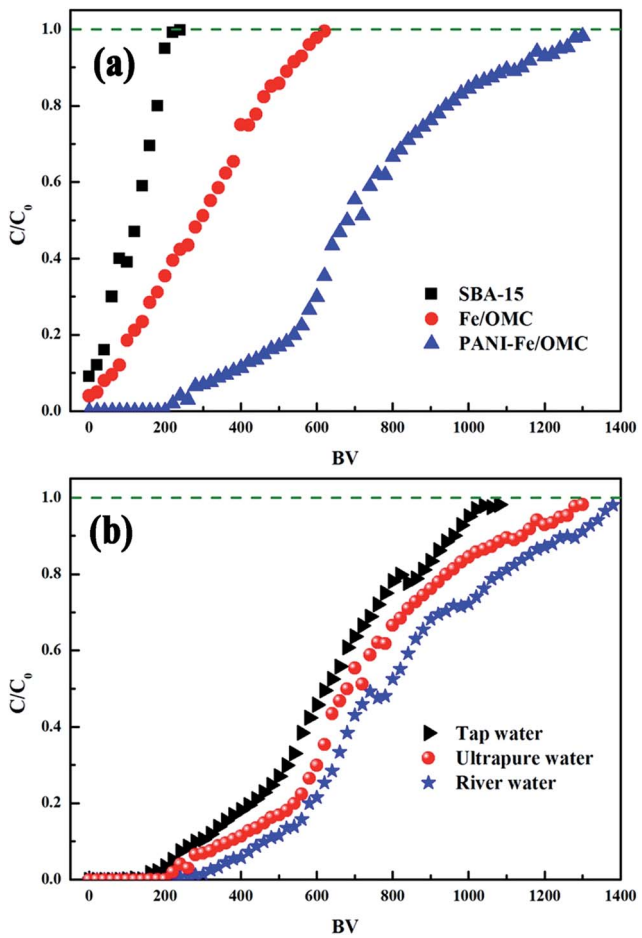

Fig. 6 Comparison of dynamic profile curves of Cr(VI) uptake onto SBA-15, Fe/OMC and PANI–Fe/OMC (a) and ultrapure water, tap water and river water (b).

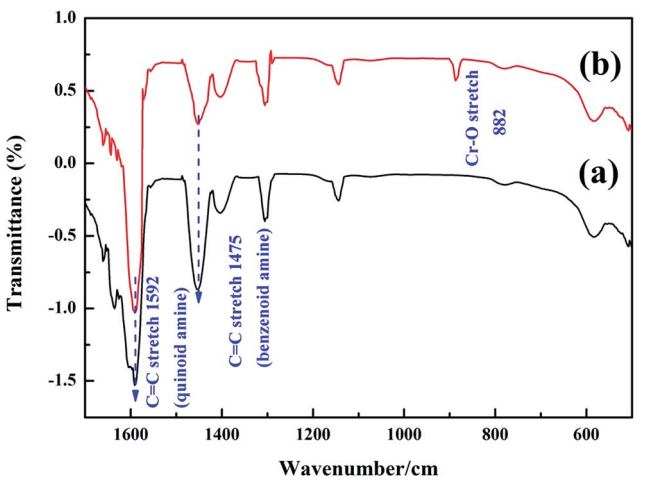

Fig. 7 FTIR spectrum of PANI–Fe/OMC before (a) and after (b) contact with Cr(VI).

whereas there was an acceleration in river water samples compared with ultrapure water. The distinct performance might be related to different co-existing substances, such as sulfate ions and phosphate ions in tap water and some common organics in river water.[41] As mentioned, these interferents could suppress or boost the uptake of Cr(VI) to some extent, respectively.

3.8 Removal mechanism

Given that the surface areas of PANI–Fe/OMC are smaller than Fe/OMC and SBA-15, the simple physical adsorption through intraparticle diffusion was eliminated, and the significant improvement in Cr(VI) uptake onto PANI–Fe/OMC is probably related to the chemical interaction at the solid/liquid interface. To gain further insights into the uptake mechanism of Cr(VI) on PANI–Fe/OMC, FTIR technique was used to analyzed the exhausted PANI–Fe/OMC. As shown in Fig. 7, the FTIR spectrum of PANI–Fe/OMC underwent several substantial changes after Cr(VI) adsorption. The increase in the peak at 1592 cm^{-1} indicates that the oxidation extent of PANI was amplified after the uptake of Cr(VI).[44] The decrease in absorption intensity at 1475 cm^{-1} suggests that some benzenoid amines of PANI have been

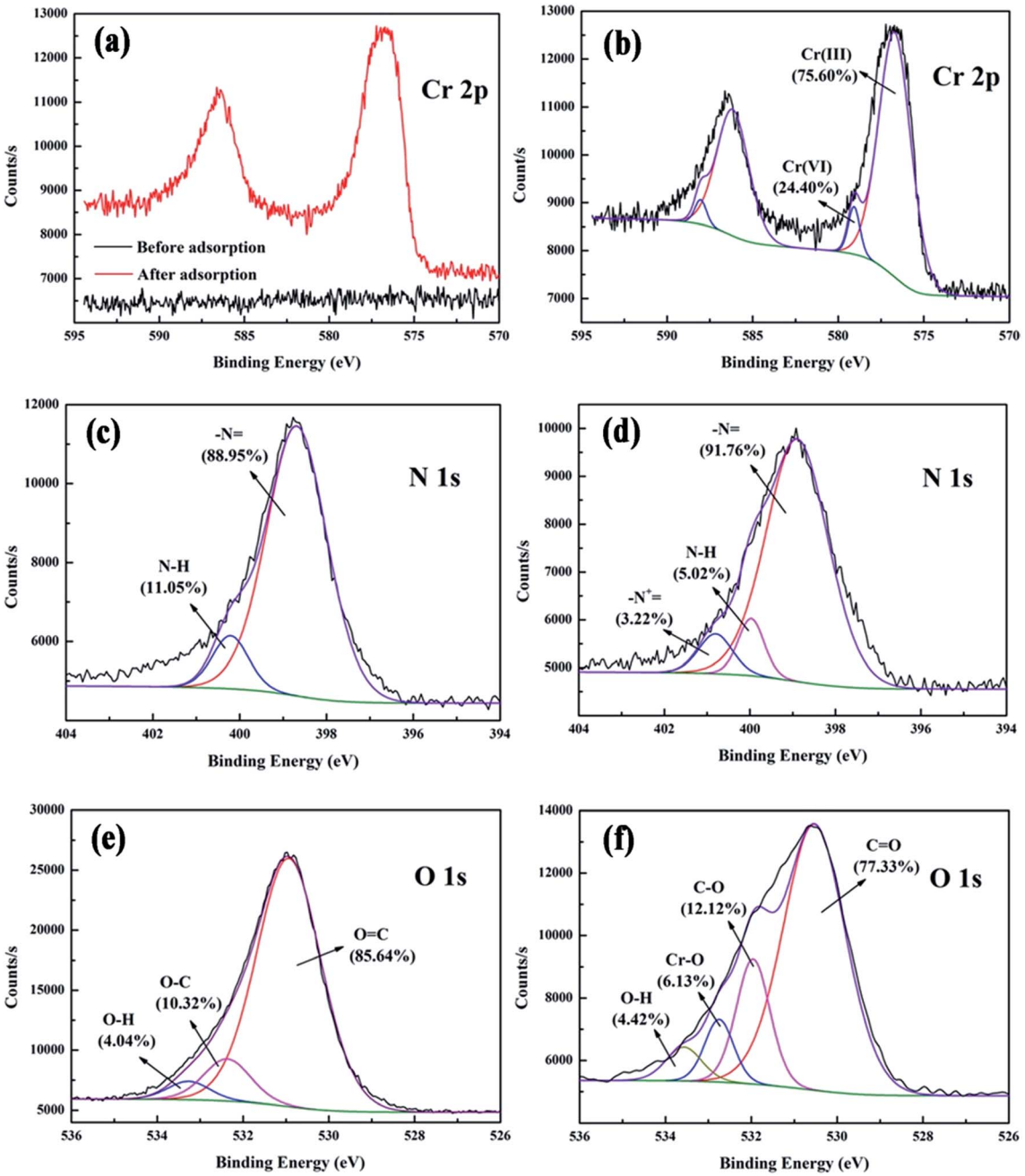

Fig. 8 XPS spectra of Cr 2p for PANI–Fe/OMC interacting with Cr(VI) (a and b). N 1s and O 1s for the PANI–Fe/OMC before (c and e) and after Cr(VI) adsorption (d and f).

oxidized from the emeraldine salt form to the pernigraniline form (quinoid amine, the highest oxidation state of PANI) during the Cr(VI) removal process.[45] The relative absorption intensity at 882 cm^{-1} for the used PANI–Fe/OMC was attributed to Cr–O mode, weaker than the characteristic infrared band of free chromate (890 cm^{-1}), which may be related to hydrogen bonding of the $HCrO_4^-$ with interlayer water molecules or layer hydroxyl groups.

Moreover, XPS spectra of PANI–Fe/OMC surfaces before and after Cr(VI) interaction were studied to elaborate the uptake process of Cr(VI). The chromium region is been determined by XPS and the results were shown in Fig. 8a and b. After interaction with Cr(VI), the binding energies at 576.4 and 578.6 eV can be assigned to Cr(III) and Cr(VI), respectively. This suggests that both Cr(VI) and Cr(III) coexist on the surface of Cr(VI)-adsorbed PANI–Fe/OMC. High-resolution spectra of N 1s showed that before Cr(VI) uptake, the N 1s region showed two distinct peaks at 398.3 and 399.2 eV, corresponding to nitrogen atoms in quinoid amine (–N=) and benzoid amine (N–H), respectively (Fig. 8c).[46] After reaction with Cr(VI), the reduced nitrogen (N–H) sharply decreased from 11.05% to 5.02%, while there was a corresponding increase in oxidated nitrogen (–N=) from 88.95% to 91.76% (Fig. 8d). This further demonstrated the redox reaction occurring between Cr(VI) and the nitrogen atoms of PANI functional groups. Meanwhile, a new peak occurred at 401.2 eV, corresponding to nitrogen atoms in doped imine ($-N^+=$). This was probably due to the sharing of electrons between nitrogen atoms and chromium, which confirmed the fixation of Cr(VI) and chelation of Cr(III) onto the PANI–Fe/OMC. The O 1s spectra of the PANI–Fe/OMC before and after interaction with Cr(VI) are shown in Fig. 8e and f. The broad peak of O 1s could be fitted by three peaks at binding energies of 530.8, 532.2 and 533.3 eV, assigned to the oxygen atoms in O=C, O–C and O–H bonds, respectively.[47] After Cr(VI) adsorption, a significant binding energy at 532.7 eV could be assigned oxygen in the Cr–O bond, which indicated that oxygen atoms also participate in the chelation of Cr(III). The C 1s and Fe 2p spectra of the PANI–Fe/OMC before and after interaction with Cr(VI) are shown in Fig. S2c–f.† The C 1s spectra (Fig. S2c and d†) were considered in the forms of C–C (283.7 eV), C–N (285.2 eV), and C–O (286.8 eV), respectively. The Fe 2p spectra (Fig. S2e and f†) were in the forms of FeO (709.6 eV) and Fe_2O_3 (711.2 eV). As can be seen, no significant changes were observed in the two spectra before and after interaction with Cr(VI), indicating that carbon and iron atoms do not interfere with the uptake of Cr(VI).

On the basis of the above analyses, the main reaction proceeding between Cr(VI) and the PANI–Fe/OMC is proposed in Fig. 9. First, the amine groups on the adsorbent are protonated under the acidic conditions, and thus the surface complexation occurred between protonated functional groups and aqueous Cr(VI) oxyanions *via* electrostatic attraction. Then, because of its strong oxidation ability, the adsorbed Cr(VI) can react with a reduced state of PANI compositions (benzenoid amines) with the assistance of hydrogen ions. The result is that the benzenoid amines are oxidised to quinoid amine, the highest oxidation state of PANI, and some Cr(VI) oxyanions were reduced to Cr(III) cations. Finally, partial Cr(III) cations were strongly fixed with the oxidated quinoid amines of PANI functional groups.

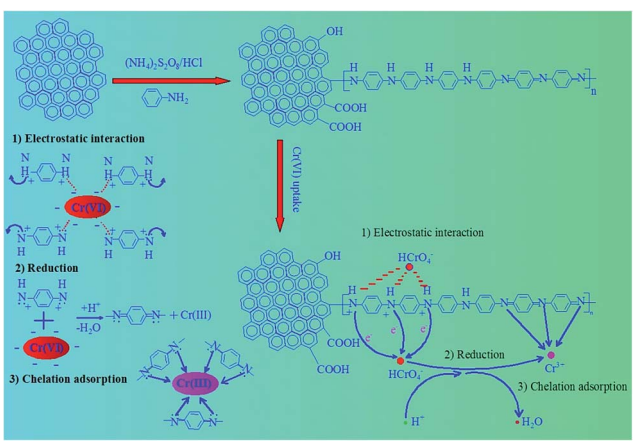

Fig. 9 Schematic for the adsorption-couple reduction mechanisms behind the removal of Cr(VI) by PANI–Fe/OMC.

4. Conclusion

In summary, a novel adsorbent PANI–Fe/OMC nanoparticles with magnetic separability were synthesized and effectively removed Cr(VI) from water. The resultant nanoparticles demonstrated a high adsorption capacity and fast rate for Cr(VI) removal. Kinetics demonstrated the adsorption capacity of PANI–Fe/OMC was obviously improved up to 2- and 10-fold compared with SBA-15 and Fe/OMC. The maximum adsorption capacity occurred at pH 2.0 and the adsorption data can be better fitted by Langmuir model. Thermodynamics revealed that the Cr(VI) adsorption is an endothermic and spontaneous natural process. Other common coexisting ions had limited influence on the adsorption capacity, while the coexisting organic interferents showed an acceleration and then suppression of Cr(VI) removal with initially increasing concentrations of HA and FA. Fixed-bed column experiments demonstrated that modified magnetic mesoporous carbon is greatly superior over other mesoporous adsorbents and could be well applied in actual chromium contamination treatment. Regeneration and reuse indicated that PANI–Fe/OMC could be well regenerated and maintained over 90% Cr(VI) adsorption efficiency in the seventh cycle. Further investigation by the comparison of FTIR and XPS spectra before and after adsorption indicated that Cr(VI) removal by PANI–Fe/OMC was an adsorption-coupled reduction process for the existence of Cr(III) and the change of nitrogen atoms in functional groups. Results from this study demonstrate the resultant PANI–Fe/OMC nanoparticle can be used as a potential novel candidate for the removal of Cr(VI) from wastewater.

Acknowledgements

The study was financially supported by the Program for the Young Top-Notch Talent Support Program of China (2012), the National Natural Science Foundation of China (51222805), the Program for New Century Excellent Talents in University from

the Ministry of Education of China (NCET-11-0129), the Fundamental Research Funds for the Central Universities, Hunan University, China, and the Foundation for the Author of Excellent Doctoral Dissertation of Hunan Province, China.

References

1 C. Kantar, Z. Cetin and H. Demiray, *J. Hazard. Mater.*, 2008, **159**, 287–293.
2 M. D. Nazime, K. Cetin, G. Sibel, J. D. Cleveland, C. Y. Banu and A. M. Mehmet, *Environ. Sci. Technol.*, 2011, **45**, 2278–2285.
3 S. Binoy, N. Ravi, S. K. Gummuluru and M. Mallavarapu, *Environ. Sci. Technol.*, 2013, **47**(23), 13629–13636.
4 Y. C. Zhang, J. Li, M. Zhang and D. D. Dionysiou, *Environ. Sci. Technol.*, 2011, **45**, 9324–9331.
5 D. Lin, S. Zhou, L. Bing, L. F. Yang, L. Lu and X. Z. Yang, *Ind. Eng. Chem. Res.*, 2014, **53**(18), 7746–7757.
6 L. Giehyeon, P. Jaeseon and R. H. Omar, *Water Res.*, 2013, **47**, 1136–1146.
7 X. H. Pan, Z. J. Liu, Z. Chen, Y. J. Cheng, D. M. Pan, J. N. Shao, Z. Lin and X. Guan, *Water Res.*, 2014, **55**, 21–29.
8 L. Alvarado, I. R. Torres and A. C. Chen, *Sep. Purif. Technol.*, 2013, **105**, 55–62.
9 L. Tang, G. D. Yang, G. M. Zeng, Y. Cai, S. S. Li, Y. Y. Zhou, Y. Pang, Y. Y. Liu, Y. Zhang and B. Luna, *Chem. Eng. J.*, 2014, **239**, 114–122.
10 X. F. Sun, Y. Ma, X. W. Liu, S. G. Wang, B. Y. Gao and X. M. Li, *Water Res.*, 2010, **44**, 2517–2524.
11 L. Y. Chai, Y. Y. Wang, N. Zhao, W. C. Yang and X. Y. You, *Water Res.*, 2013, **47**, 4040–4049.
12 Y. Y. Sun, Q. Y. Yue, B. Y. Gao, Y. Gao, Q. Li and Y. Wang, *Chem. Eng. J.*, 2013, **217**, 240–247.
13 Y. X. Zhao, S. J. Yang, D. H. Ding, J. Chen, Y. N. Yang, Z. F. Lei, C. P. Feng and Z. Y. Zhang, *J. Colloid Interface Sci.*, 2013, **395**, 198–204.
14 M. R. Gandhi and S. Meenakshi, *Carbohydr. Polym.*, 2013, **91**, 631–637.
15 L. Tang, Y. Cai, G. D. Yang, Y. Y. Liu, G. M. Zeng, Y. Y. Zhou, S. S. Li, J. J. Wang, S. Zhang, Y. Fang and Y. B. He, *Appl. Surf. Sci.*, 2014, **314**, 746–753.
16 L. Tang, Y. Fang, Y. Pang, G. M. Zeng, J. J. Wang, Y. Y. Zhou, Y. C. Deng, G. D. Yang, Y. Cai and J. Chen, *Chem. Eng. J.*, 2014, **254**, 302–312.
17 P. Wang and I. M. C. Lo, *Water Res.*, 2009, **43**, 3727–3734.
18 L. J. Xu and J. L. Wang, *Environ. Sci. Technol.*, 2012, **46**, 10145–10153.
19 X. Guo, G. T. Fei, H. Su and L. D. Zhang, *J. Phys. Chem. C*, 2011, **115**, 1608–1613.
20 Y. Yang, M. H. Diao, M. M. Gao, X. F. Sun, X. W. Liu, G. H. Zhang, Z. Qi and S. G. Wang, *Electrochim. Acta*, 2014, **132**, 496–503.
21 D. Y. Zhao, J. L. Feng, Q. S. Huo, N. G. Melosh, H. Fredrickson, B. F. Chmelka and G. D. Stucky, *Science*, 1998, **279**, 548–552.
22 X. F. Wang, P. Liu, Y. Tian and L. Q. Zang, *Microporous Mesoporous Mater.*, 2011, **145**, 98–103.
23 Z. B. Lei, X. X. Sun, H. J. Wang, Z. H. Liu and X. S. Zhao, *ACS Appl. Mater. Interfaces*, 2013, **5**, 7501–7508.
24 B. Yuan, X. F. Wu, Y. X. Chen, J. H. Huang, H. M. Luo and S. G. Deng, *Environ. Sci. Technol.*, 2013, **47**, 5474–5480.
25 W. Teng, Z. X. Wu, D. Feng, J. W. Fan, J. X. Wang, H. Wei, M. J. Song and D. Y. Zhao, *Environ. Sci. Technol.*, 2013, **47**, 8633–8641.
26 J. Yang, J. X. Wu, Q. F. Lü and T. T. Lin, *ACS Sustainable Chem. Eng.*, 2014, **2**, 1203–1211.
27 G. D. Yang, L. Tang, X. X. Lei, G. M. Zeng, Y. Cai, X. Wei, Y. Y. Zhou, S. S. Li, Y. Fang and Y. Zhang, *Appl. Surf. Sci.*, 2014, **292**, 710–716.
28 J. H. Zhu, S. Y. Wei, H. B. Gu, S. B. Rapole, Q. Wang, Z. P. Luo, N. Haldolaarachchige, D. P. Young and Z. H. Guo, *Environ. Sci. Technol.*, 2012, **46**, 977–985.
29 G. X. Yang and H. Jiang, *Water Res.*, 2014, **48**, 396–405.
30 Y. Li, S. M. Zhu, Q. L. Liu, Z. X. Chen, J. J. Gu, C. L. Zhu, T. Lu, D. Zhang and J. Ma, *Water Res.*, 2013, **47**, 4188–4197.
31 Y. J. Lia, B. Y. Gao, T. Wu, D. J. Sun, X. Li, B. Wang and F. J. Lu, *Water Res.*, 2009, **43**, 3067–3075.
32 Z. H. Ai, Y. Cheng, L. Z. Zhang and J. R. Qiu, *Environ. Sci. Technol.*, 2008, **42**, 6955–6960.
33 Y. Pang, G. M. Zeng, L. Tang, Y. Zhang, Y. Y. Liu, X. X. Lei, Z. Li, J. C. Zhang, Z. F. Liu and Y. Q. Xiong, *Chem. Eng. J.*, 2011, **175**, 222–227.
34 A. G. Yavuz, E. Dincturk-Atalay, A. Uygun, F. Gode and E. Aslan, *Desalination*, 2011, **279**, 325–331.
35 V. K. Gupta, D. Pathania, S. Sharma and P. J. Singh, *Colloids Interface Sci.*, 2013, **401**, 125–132.
36 M. Anbia, K. Kargosha and S. Khoshbooei, *Chem. Eng. Res. Des.*, 2014, DOI: 10.1016/j.cherd.2014.07.018.
37 W. Q. Cai, L. J. Tan, J. G. Yu, M. Jaroniec, X. Q. Liu, B. Cheng and F. Verpoort, *Chem. Eng. J.*, 2014, **239**, 207–215.
38 J. Zhu, H. Gu, J. Guo, M. Chen, H. Wei, Z. Luo, H. A. Colorado, N. Yerra, D. Ding, T. C. Ho, N. Haldolaarachchige, J. Hopper, D. P. Young, Z. Guo and S. Wei, *J. Mater. Chem. A*, 2014, **2**, 2256–2265.
39 E. Petala, K. Dimos, A. Douvalis, T. Bakas, J. Tucek, R. Zbořil and M. A. Karakassides, *J. Hazard. Mater.*, 2013, **261**, 295–306.
40 L. N. Shi, X. Zhang and Z. L. Chen, *Water Res.*, 2011, **45**, 886–892.
41 O. Hakami, Y. Zhang and C. J. Banks, *Water Res.*, 2012, **46**, 3913–3922.
42 P. L. Younger, *Blackwell Publishing Ltd.*, Main Street, Malden, MA, USA, 2007.
43 J. K. Yang and S. M. Lee, *Chemosphere*, 2006, **63**, 1677–1684.
44 W. T. Yu, L. Y. Zhang, H. Y. Wang and L. Y. Chai, *J. Hazard. Mater.*, 2013, **260**, 789–795.
45 J. Wang, K. K. Zhang and L. Zhao, *Chem. Eng. J.*, 2014, **239**, 123–131.
46 Y. Zhang, Q. Li, L. Sun, R. Tang and J. P. Zhai, *J. Hazard. Mater.*, 2010, **175**, 404–409.
47 Z. X. Wu, W. Li, P. A. Webley and D. Y. Zhao, *Adv. Mater.*, 2012, **24**, 485–491.